Molecular Raman effect in the optical microcavity: QED vacuum confinement of an inelastic quantum scattering process

F. De Martini, M. Marrocco,* C. Pastina, and F. Viti
Dipartimento di Fisica dell'Università "La Sapienza" and Istituto Nazionale di Fisica Nucleare, 00185 Rome, Italy
(Received 12 April 1995)

The spontaneous Raman scattering from liquid samples of C_6H_6 is investigated in the Casimir topology of a microscopic optical Fabry-Pérot cavity terminated by Bragg reflectors tuned at the emitted Stokes wavelength. The given general quantum scattering theory is based on a complete set of mode functions describing the cavity-confined field in its vacuum state. The coupling of the field with the normal CH ring stretching mode at $\Delta\nu = 3062$ cm^{-1} (totally symmetric species A_{1g}) of the benzene molecule is given via the related Raman tensor, which leads to the appropriate form of the coupling Hamiltonian. A detailed experimental investigation of the spontaneous Raman scattering for the mode is then reported. The results confirm the relevant predictions of the scattering theory, namely, the effect of the vacuum confinement on the enhancement and inhibition of the *total* and *differential cross sections*, on the *angular distribution* of the scattered radiation, and on the *molecular depolarization ratio*.

PACS number(s): 42.62.Fi, 42.65.Dr

I. INTRODUCTION

Scattering is a most fundamental concept of modern physics as it concerns all kinds of quantum interactions, at any energy of the particles involved. For any such process the key parameter accessible through the S-matrix formulation is the scattering cross section σ and the differential cross section $d\sigma/d\Omega$ [1]. These parameters are generally thought of as expressing the space-time local properties of the interacting quantum particles. In the present work we give the experimental demonstration, in the context of a basic spontaneous scattering process of molecular spectroscopy, that the above parameters, as well as other relevant scattering parameters (e.g., the molecular depolarization ratio), are in fact highly sensitive to *nonlocal* properties of the photon field at optical frequencies. In our work this is obtained experimentally by the confinement of the scattering process within the structures of an optical microcavity terminated by dielectric mirrors.

Since the early years of quantum electrodynamics, it has been common knowledge that the spontaneous-emission rate of an atomic source depends on the structure of the vacuum-field modes surrounding the atom [2]. It is also well known that this structure can be strongly modified by appropriate electromagnetic boundaries (single mirror or cavities) and over the past decades a great deal of theoretical effort has been devoted to this process [3]. In more recent times, most of the theoretical predictions have been confirmed by several experiments on atomic spontaneous emission in the microwave and infrared frequency range [4]. In the optical domain the confinement process has been investigated by the use of single mirrors [5] and, more recently, of the optical microcavity [6].

The present work provides a demonstration that these concepts, investigated so far in the limited domain of the atomic spontaneous emission, are in fact relevant in the framework of any QED scattering process. In order to fulfill this program, we have selected as a paradigmatic example the case of an inelastic light-scattering process at optical frequencies: The Raman effect [7]. In order to emphasize the basic principle, we have also selected the benzene molecule (C_6H_6) as the active Raman medium. This well-known molecule is generally considered, within the paradigm of molecular spectroscopy, as a typical source to demonstrate the basic features of Raman scattering [8]. In this respect, the present work also establishes a spectroscopic method and provides information of specific relevance in the domain of molecular spectroscopy.

More precisely, we report an extensive study of the Raman scattering process in benzene in the condition of strong confinement of the Stokes field by a plane, Fabry-Pérot microcavity, with the cavity order $m = 2d/\lambda \equiv d/d = (\text{whole number}) \geqslant 1$, d being the cavity effective spacing and λ the Stokes wavelength [9]. The anomalous behavior of σ, $d\sigma/d\Omega$, and the molecular depolarization ratio related to cavity-confined scattering will be investigated theoretically and experimentally by direct comparison with the free-space values.

The present work is organized as follows. Section II derives the traveling electromagnetic wave modes of the cavity. Our calculations are based on a complete set of spatial modes that cover all the space, including the interior of the cavity and the exterior regions that extend to infinite distances on either side. The radiation field is then quantized in terms of these modes in Sec. III. The scattering parameters, i.e., the cross section and the depolarization ratio, for a Stokes transition are derived in Secs. IV and V, respectively. The effect of the random orientations of the molecules on the scattering parameters is considered in Sec. V. The problem is then specified for the case of the benzene molecule in Sec. VI, whereas Secs. VII and VIII report the experimental setup and the complete set of the results, respectively.

II. TRAVELING-WAVE MODELS OF A FABRY-PÉROT CAVITY

In order to calculate the spontaneous Raman scattering cross section in a Fabry-Pérot cavity, we first determine the

*Present address: Max-Planck-Institut für Quantenoptik, D-85748 Garching, Germany.

appropriate complete set of spatial modes for quantization of the electromagnetic field [10]. Refer to Fig. 1: the z axis is taken normal to the mirrors with its origin in the middle of the cavity. The mirrors are assumed to have infinite extents in the x-y plane. As shown in Fig. 1, multiple reflections to the field couple together waves of wave vectors

$$\mathbf{k}_+ = k(\sin\theta\cos\phi, \sin\theta\sin\phi, \cos\theta), \tag{2.1}$$

$$\mathbf{k}_- = k(\sin\theta\cos\phi, \sin\theta\sin\phi, -\cos\theta) \tag{2.2}$$

for $(0 \leqslant \theta \leqslant \frac{1}{2}\pi)$. Four distinct spatial modes can be constructed from contributions with the same two wave vectors. For each set of polar angles θ and ϕ, there are two transverse polarization directions whose unit vectors are chosen to be

$$\boldsymbol{\varepsilon}(\mathbf{k}_+, 1) = \boldsymbol{\varepsilon}(\mathbf{k}_-, 1) = (\sin\phi, -\cos\phi, 0), \tag{2.3}$$

$$\boldsymbol{\varepsilon}(\mathbf{k}_+, 2) = (\cos\theta\cos\phi, \cos\theta\sin\phi, -\sin\theta),$$

$$\boldsymbol{\varepsilon}(\mathbf{k}_-, 2) = (\cos\theta\cos\phi, \cos\theta\sin\phi, \sin\theta), \tag{2.4}$$

where the $\mathbf{k}_+$ and $\mathbf{k}_-$ designations indicate the polarizations of the respective wave-vector contributions. It is convenient to indicate the polarizations (2.3) and (2.4) by an index $j = 1,2$. The complex reflection and transmission coefficients r_{1j}, t_{1j} and r_{2j}, t_{2j} of the cavity mirrors are generally different for the two polarizations and depend on the polar angle θ. They are assumed to have the following unitary lossless properties for values of θ:

$$|r_{1j}|^2 + |t_{1j}|^2 = |r_{2j}|^2 + |t_{2j}|^2 = 1, \tag{2.5}$$

$$r_{1j}^* t_{1j} + r_{1j} t_{1j}^* = r_{2j}^* t_{2j} + r_{2j} t_{2j}^* = 0, \tag{2.6}$$

where r_{ij}^*, t_{ij}^* are complex conjugates of r_{ij}, t_{ij}. Optical propagation within the mirrors is not important for the present study and we accordingly ignore their internal mode structures. For each pair of coupled wave vectors $\mathbf{k}_+, \mathbf{k}_-$, designed by $\mathbf{k}$ for brevity, and for each transverse polarization there are two distinct mode functions corresponding to incoming plane waves of unit amplitude that are incident, respectively, from the negative- and positive-z sides of the cavity. The forms of these functions are obtained, as usual in Fabry-Pérot theory, by summing the geometric series resulting from the multiple reflections at the mirrors placed at the mutual distance d. The two kinds of spatial dependence are thus given as follows:

Mode function $U_{kj}(\mathbf{r})$

$\mathbf{k}_+$	$\mathbf{k}_-$	z
$\exp(i\mathbf{k}_+ \cdot \mathbf{r})$	$R_{kj} \exp(i\mathbf{k}_- \cdot \mathbf{r})$	$-\infty < z < -\frac{d}{2}$
$t_{1j} \exp(i\mathbf{k}_+ \cdot \mathbf{r})/D_j$	$t_{1j} r_{2j} \exp(i\mathbf{k}_- \cdot \mathbf{r} + ikd\cos\theta)/D_j$	$-\frac{d}{2} < z < +\frac{d}{2}$
$T_{kj} \exp(i\mathbf{k}_+ \cdot \mathbf{r})$	0	$\frac{d}{2} < z < +\infty$

(2.7)

Mode function $U'_{kj}(\mathbf{r})$

$\mathbf{k}_-$	$\mathbf{k}_+$	z
$T'_{kj} \exp(i\mathbf{k}_- \cdot \mathbf{r})$	0	$-\infty < z < -\frac{d}{2}$
$t_{2j} \exp(i\mathbf{k}_- \cdot \mathbf{r})/D_j$	$t_{2j} r_{1j} \exp(i\mathbf{k}_+ \cdot \mathbf{r} + ikd\cos\theta)/D_j$	$-\frac{d}{2} < z < +\frac{d}{2}$
$\exp(i\mathbf{k}_- \cdot \mathbf{r})$	$R_{kj} \exp(i\mathbf{k}_+ \cdot \mathbf{r})$	$\frac{d}{2} < z < +\infty$

(2.8)

where the expressions in each row of (2.7) and (2.8) represent, as shown in Fig. 1, the plane-wave mode functions propagating in the space portions indicated at the right-hand side and excited for the sets U_{kj} and U'_{kj} by the waves $\exp(i\mathbf{k}_+ \cdot \mathbf{r})$ and $\exp(i\mathbf{k}_- \cdot \mathbf{r})$, respectively. In (2.7) and (2.8) the various quantities are defined as

$$D_j \equiv 1 - r_{1j} r_{2j} \exp(2ikd\cos\theta), \tag{2.9}$$

$$R_{kj} \equiv [r_{ij} \exp(-ikd\cos\theta) + r_{2j}(t_{1j}^2 - r_{1j}^2) \times \exp(ikd\cos\theta)]/D_j, \tag{2.10}$$

$$T_{kj} = T'_{kj} \equiv t_{1j} t_{2j}/D_j, \tag{2.11}$$

$$R'_{kj} \equiv [r_{2j} \exp(-ikd\cos\theta) + r_{1j}(t_{2j}^2 - r_{2j}^2) \times \exp(ikd\cos\theta)]/D_j. \tag{2.12}$$

The last three quantities represent the reflection and transmission coefficients of the cavity as a whole. With the use of (2.5) and (2.6) they satisfy

$$|R_{kj}| = |R'_{kj}|, \tag{2.13}$$

$$|R_{kj}|^2 + |T_{kj}|^2 = |R'_{kj}|^2 + |T'_{kj}|^2 = 1, \tag{2.14}$$

$$R_{kj}^* T'_{kj} + R'_{kj} T_{kj}^* = 0. \tag{2.15}$$

These properties ensure the normalization and orthogonality of the two modes that have the same wave vector and polarizations and the general relations are

$$\int d\mathbf{r}\ \boldsymbol{\varepsilon}(\mathbf{k}, j) \cdot \boldsymbol{\varepsilon}(\mathbf{k}', j') U_{\mathbf{k}j}(\mathbf{r}) U'^*_{\mathbf{k}'j'}(\mathbf{r}) = 0, \tag{2.16}$$

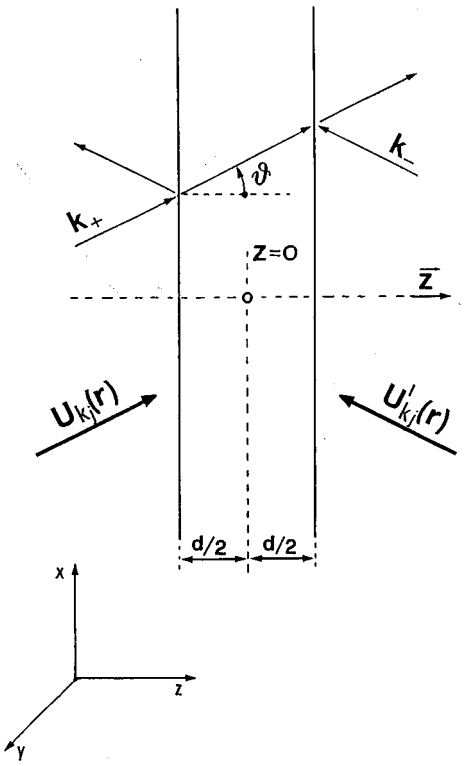

FIG. 1. Geometry of the Fabry-Pérot microcavity showing the two kinds of modes $\mathbf{k}_+$ and $\mathbf{k}_-$. Mirrors labeled by 1 and 2 in the text are represented, respectively, on the left and right in the figure.

$$\int d\mathbf{r}\ \boldsymbol{\varepsilon}(\mathbf{k},j)\cdot\boldsymbol{\varepsilon}(\mathbf{k}',j')U_{\mathbf{k}j}(\mathbf{r})U^{*}_{\mathbf{k}'j'}(\mathbf{r}) = 2\pi\delta_{ij'}\delta(\mathbf{k}-\mathbf{k}'), \tag{2.17}$$

together with the identical normalization integral for the primed mode function (2.8). The modes (2.7) and (2.8) form a complete set of functions for all the space, including the interior of the cavity and the exterior regions on either side. They allow calculations to be made of the spontaneous-emission rates for the atoms that are excited in cavities whose mirrors both transmit nonzero fractions of the emitted intensity. Likewise, this set of modes is taken as the basis of our quantum-dynamical approach in the present work on Raman scattering. In the limiting case of a perfectly reflecting closed cavity, the traveling-wave mode functions used here reproduce results ordinarily obtained with standing-wave modes, while in the opposite extreme of an absent cavity, the mode functions (2.7) and (2.8) taken together produce the usual complete set of plane waves in infinite free space. In intermediate conditions the modes form a convenient basis for general calculations and they are free of the potential limitations inherent in modes restricted to exterior regions of finite extent or to only one side of the cavity.

III. FIELD QUANTIZATION AND INTERACTION HAMILTONIAN

The electromagnetic field is quantized by the introduction of the mode creation and destruction operators. The operators for the modes with spatial functions U_{kj} and U'_{kj} are denoted by $\hat{a}^{\dagger}_{\mathbf{k}j},\hat{a}_{\mathbf{k}j}$ and $\hat{a}'^{\dagger}_{\mathbf{k}j},\hat{a}'_{\mathbf{k}j}$, respectively, where $j=1,2$ indicates the choice of mode polarization (2.3) or (2.4). With $\mathbf{k}$ taken to be a continuous variable, the operators satisfy the commutation relations

$$[\hat{a}_{\mathbf{k}j},\hat{a}^{\dagger}_{\mathbf{k}'j'}]=[a_{\mathbf{k}j},\hat{a}^{\dagger}_{\mathbf{k}'j'}]=\delta_{jj'}\delta(\mathbf{k}-\mathbf{k}'),$$
$$[\hat{a}_{\mathbf{k}j},\hat{a}^{\dagger}_{\mathbf{k}'j'}]=[\hat{a}'_{\mathbf{k}j},\hat{a}^{\dagger}_{\mathbf{k}'j'}]=0. \tag{3.1}$$

The electromagnetic-field quantization now proceeds in the usual way [11] and we quote only the main results.

The interaction Hamiltonian for the radiation field, the electrons, and the nuclei of the molecule may be expressed by the sum

$$\hat{H}_T=\hat{H}_{ER}+\hat{H}_{EV}, \tag{3.2}$$

where $\hat{H}_{ER}$ is the Hamiltonian for the interaction in the cavity of the electrons with the electromagnetic field at the Raman-Stokes frequency $\omega=ck$ and wavelength $\lambda=2\pi/k$ and with the incident field with frequency $\omega_i=ck_i$ and polarization $\boldsymbol{\varepsilon}_i$. The microcavity mirror reflectivities are such that *only* the Stokes radiation is confined. $\hat{H}_{EV}$ is the Hamiltonian for the interaction between the electrons and vibrational motion of the molecule. The explicit form of the first contribution in (3.2) is given by the sum of two terms, corresponding to the two different fields

$$\hat{H}_{ER}=\hat{H}_i+\hat{H}, \tag{3.3}$$

with

$$\hat{H}_i=i\left(\frac{\hbar ck_i}{2\varepsilon_0 V}\right)^{1/2}\hat{a}^{\dagger}_{i\mathbf{k}i}\boldsymbol{\varepsilon}_i\cdot\hat{\boldsymbol{\mu}}\ \exp(-i\mathbf{k}_i\cdot\mathbf{r})+\text{H.c.} \tag{3.4}$$

for the incident field having the polarization $\boldsymbol{\varepsilon}_i$ that is orthogonal to the z axis and makes an angle ψ with the vertical axis x. The interaction Hamiltonian is

$$\begin{aligned}\hat{H}=i\int d\mathbf{k}\sum_p\left(\frac{\hbar ck}{16\pi^3\varepsilon_0}\right)^{1/2}\frac{1}{D_j}\{&t_{1j}[\boldsymbol{\varepsilon}(\mathbf{k}_+,j)\exp(-i\mathbf{k}_+\cdot\mathbf{r})\\&+\boldsymbol{\varepsilon}(\mathbf{k}_-,j)r_{2j}\ \exp(-i\mathbf{k}_-\cdot\mathbf{r}-ikd\ \cos\theta)]\hat{a}^{\dagger}_{\mathbf{k}_j}\\&+t_{2j}[\boldsymbol{\varepsilon}(\mathbf{k}_-,j)\ \exp(-i\mathbf{k}_-\cdot\mathbf{r})+\boldsymbol{\varepsilon}(\mathbf{k}_+,j)r_{1j}\\&\times\exp(-i\mathbf{k}_+\cdot\mathbf{r}-ikd\ \cos\theta)]\ \hat{a}'^{\dagger}_{kj}\}\cdot\hat{\boldsymbol{\mu}}+\text{H.c.}\end{aligned} \tag{3.5}$$

for the vacuum stokes field, where $\mathbf{r}$ is the space vector inside the cavity indicating the position of the molecule and $\hat{\boldsymbol{\mu}}$ is the dipole moment operator. $\hat{a}_{\mathbf{k}j}$ and $\hat{a}_{i\mathbf{k}_i}$ are single-mode Bose operators representing the electromagnetic fields at the Stokes and incident (pump) frequencies, respectively. The vibrational contribution is given by the first-order approximation of the Coulomb energy changes due to the relative motions of the nuclei with respect to the electrons. If Q_a indicates the normal coordinates of the nuclei, then this contribution is [12]

$$\hat{H}_{EV}=\sum_a\ \hat{\kappa}_a\hat{Q}_a, \tag{3.6}$$

the sum runs over the possible molecule vibrations of frequency Ω_a, and

$$\hat{\kappa}_a=\left(\frac{\partial \hat{H}_{\mathrm{Coul}}}{\partial Q_a}\right)_0=-\frac{e}{4\pi\varepsilon_0}\sum_{l,\sigma}\left(\frac{\partial(Z_\sigma/r_{l\sigma})}{\partial Q_a}\right)_0 \tag{3.7}$$

is the operator that mixes the electronic states, where e is the electronic charge, Z_σ the charge of the nucleus σ, and $r_{1\sigma}$ the distance between the electron l and the nucleus σ. The index 0 means that the derivatives have to be taken at the equilibrium configuration of the molecule. The normal coordinate operator $\hat{Q}_a$ is given in the quantum-mechanical description of the harmonic oscillator by

$$\hat{Q}_a=\left(\frac{\hbar}{2\Omega_a}\right)^{1/2}(\hat{b}_a^\dagger+\hat{b}_a), \tag{3.8}$$

where $\hat{b}_a^\dagger,\hat{b}_a$ corresponds to the Bose creation and destruction operators of the vibrational mode a. Hence the Hamiltonian (3.6) becomes [13]

$$\hat{H}_{EV}=\sum_a\left(\frac{\hbar}{2\Omega_a}\right)^{1/2}\hat{\kappa}_a(\hat{b}_a^\dagger+\hat{b}_a). \tag{3.9}$$

In (3.2) both Stokes and anti-Stokes processes are included. The suitable combinations of the operators contained in the overall Hamiltonian are

$$(\hat{a}_{i\mathbf{k}_i},\hat{a}_{\mathbf{k}j}^\dagger \quad \text{or} \quad \hat{a}_{\mathbf{k}j}'^\dagger,\hat{b}_a^\dagger)\rightarrow\text{Stokes transition}, \tag{3.10}$$

$$(\hat{a}_{i\mathbf{k}_i},\hat{a}_{\mathbf{k}j}^\dagger \quad \text{or} \quad \hat{a}_{\mathbf{k}j}'^\dagger,\hat{b}_a)\rightarrow\text{anti-Stokes transition}. \tag{3.11}$$

The double choice for the scattered field operator means that the detector placed outside the cavity can detect the photon emitted from the molecule inside the cavity into the $\mathbf{k}_+$ or $\mathbf{k}_-$ direction. Since the present spontaneous-emission experiment deals with a Stokes process, we disregard the anti-Stokes contribution (3.11) in the rest of the paper.

IV. RAMAN SCATTERING CROSS SECTION

The spontaneous Raman scattering cross section is calculated using the time-dependent perturbation theory [14] for one molecule of the medium placed in the vacuum field of the cavity. Let us suppose that an incident excitation photon at frequency ω_i with polarization vector $\boldsymbol{\varepsilon}_i$ is annihilated and creates a scattered photon at the frequency $\omega=\omega_i-\Omega_a$ and let us call $\hat{\mathbf{R}}_a$ the 3×3 Raman tensor. The elements $R_a^{p,q}$ of $\hat{\mathbf{R}}_a$ are identified by couples of indices p and q, representing, respectively, the spatial principal axes X, Y, Z of the molecule.

The general free-space Raman scattering process for a liquid has been studied in the past by several authors, for instance, Peticolas *et al.* [13,15] and Kato and Takuma [16]. In a microcavity, the usual expression for the Raman cross section is modified by the mode structures contained in (3.5). For each polarization of the scattered radiation we may write accordingly

$$\sigma(j)=A\int\frac{1}{|D_j|^2}\{|t_{1j}|^2m_{2j}(-)+|t_{2j}|^2m_{1j}(+)\}d\Omega, \tag{4.1}$$

where $|D_j|^{-2}$ is the Airy factor of the cavity with D_j given in Eq. (2.9) and

$$A=\left(\frac{\varepsilon(\omega)}{\varepsilon(\omega_i)}\right)^{1/2}\frac{\hbar(\bar{v}+1)\omega^4L'}{2\Omega_ac^4}, \tag{4.2}$$

where $\varepsilon(\omega_i)$ and $\varepsilon(\omega)$ are the dielectric constants of the medium at ω_i and ω, respectively, c is the velocity of light, $\bar{v}=1/[\exp(\hbar\Omega_a/k_BT)-1]$ is the average quantum number of the thermally excited vibration of the chosen Raman mode, and L' is the local-field correction factor [16]. The m functions appearing in the expression of the cross section Eq. (4.1) express, in a detailed form, the interplay of the various polarization components brought about by the cavity structure. They are given by

$$\begin{aligned}m_{2j}(-)=&\{\langle[\boldsymbol{\varepsilon}(\mathbf{k}_+,j)\cdot\hat{\mathbf{R}}_a\cdot\boldsymbol{\varepsilon}_i]^2\rangle+|r_{2j}|^2\langle[\boldsymbol{\varepsilon}(\mathbf{k}_-,j)\cdot\hat{\mathbf{R}}_a\cdot\boldsymbol{\varepsilon}_i]^2\rangle\\&+2|r_{2j}|\langle[\boldsymbol{\varepsilon}(\mathbf{k}_+,j)\cdot\hat{\mathbf{R}}_a\cdot\boldsymbol{\varepsilon}_i][\boldsymbol{\varepsilon}(\mathbf{k}_-,j)\cdot\hat{\mathbf{R}}_a\cdot\boldsymbol{\varepsilon}_i]\rangle\\&\times\cos[k(d-2z)\cos\theta+\phi_{2j}]\},\end{aligned} \tag{4.3}$$

$$\begin{aligned}m_{1j}(+)=&\{\langle[\boldsymbol{\varepsilon}(\mathbf{k}_-,j)\cdot\hat{\mathbf{R}}_a\cdot\boldsymbol{\varepsilon}_i]^2\rangle+|r_{1j}|^2\langle[\boldsymbol{\varepsilon}(\mathbf{k}_+,j)\cdot\hat{\mathbf{R}}_a\cdot\boldsymbol{\varepsilon}_i]^2\rangle\\&+2|r_{1j}|\langle[\boldsymbol{\varepsilon}(\mathbf{k}_+,j)\cdot\hat{\mathbf{R}}_a\cdot\boldsymbol{\varepsilon}_i][\boldsymbol{\varepsilon}(\mathbf{k}_-,j)\cdot\hat{\mathbf{R}}_a\cdot\boldsymbol{\varepsilon}_i]\rangle\\&\times\cos[k(d+2z)\cos\theta+\phi_{1j}]\},\end{aligned} \tag{4.4}$$

where z refers to the position of the molecule in the cavity (Fig. 1) and the ϕ term is the reflection phase of the Stokes field data at the mirror. The notation $\langle\ \rangle$ refers to averages over the random orientation of the molecular axes in the medium, assumed throughout this paper to be in the liquid phase, at temperature T.

Expression (4.1) leads, upon removal of the reflecting mirrors (i.e, by taking $r_{1j}=r_{2j}=0$ and $t_{1j}=t_{2j}=1$), to the well-know formula valid in absence of any confinement [16]

$$\begin{aligned}\sigma_0(j)=A\int\{&\langle[\boldsymbol{\varepsilon}(\mathbf{k}_+,j)\cdot\hat{\mathbf{R}}_a\cdot\boldsymbol{\varepsilon}_i]^2\rangle\\&+\langle[\boldsymbol{\varepsilon}(\mathbf{k}_-,j)\cdot\hat{\mathbf{R}}_a\cdot\boldsymbol{\varepsilon}_i]^2\rangle\}d\Omega.\end{aligned} \tag{4.5}$$

At last the general expression of the relative cross section may be given in the form

$$\frac{\sigma(j)}{\sigma_0(j)}=\frac{\int\frac{1}{|D_j|^2}\{|t_{1j}|^2m_{2j}(-)+|t_{2j}|^2m_{1j}(+)\}d\Omega}{\int\{\langle[\boldsymbol{\varepsilon}(\mathbf{k}_+,j)\cdot\hat{\mathbf{R}}_a\cdot\boldsymbol{\varepsilon}_i]^2\rangle+\langle[\boldsymbol{\varepsilon}(\mathbf{k}_-,j)\cdot\boldsymbol{\varepsilon}_i]^2\rangle\}d\Omega}. \tag{4.6}$$

On the basis of this expression, representing one of the relevant results of this work, the theoretical curve of Fig. 5 has been drawn.

Note that in the simple case of a diagonal spherical tensor

$$\hat{\mathbf{R}}_a=\begin{pmatrix}\alpha&0&0\\0&\alpha&0\\0&0&\alpha\end{pmatrix} \tag{4.7}$$

we reproduce the results already obtained for the spontaneous-emission rate of a dipole with $\boldsymbol{\mu}$ oriented parallel to the mirror plane [expression (4.4) of [10]]

$$\frac{\sigma}{\sigma_0}=\frac{3}{8}\int_0^1\frac{1}{|D_1|^2}\Big(\big(|t_{11}|^2\{1+|r_{21}|^2+2|r_{21}|\cos[k(d-2z)\cos\theta+\phi_{21}]\}+|t_{21}|^2\{1+|r_{11}|^2+2|r_{11}|\cos[k(d+2z)\cos\theta+\phi_{11}]\}\big)$$
$$+\frac{1}{|D_2|^2}C^2\big(|t_{12}|^2\{1+|r_{22}|^2+2|r_{22}|\cos[k(d-2z)\cos\theta+\phi_{22}]\}+|t_{22}|^2\{1+|r_{12}|^2+2|r_{12}\cos[k(d+2z)\cos\theta$$
$$+\phi_{12}]\}\big)\Big)dC. \tag{4.8}$$

It can be easily proved that this very particular symmetry of the Raman tensor $\hat{\mathbf{R}}_a$ leads to the maximum value of the scattering enhancement due to the cavity confinement.

V. RAMAN TENSOR: MEAN VALUES AND THE DEPOLARIZATION RATIO

We turn now our attention to the averages that appear in (4.3) and (4.4). Their explicit forms are

$$\langle[\boldsymbol{\varepsilon}(\mathbf{k}_+,j)\cdot\hat{\mathbf{R}}_a\cdot\boldsymbol{\varepsilon}_i]^2\rangle=\left\langle\left(\sum_{\lambda,\mu}[\boldsymbol{\varepsilon}(\mathbf{k}_+,j)]_\lambda R_a^{\lambda\mu}[\boldsymbol{\varepsilon}_i]_\mu\right)^2\right\rangle, \tag{5.1}$$

$$\langle[\boldsymbol{\varepsilon}(\mathbf{k}_-,j)\cdot\hat{\mathbf{R}}_a\cdot\boldsymbol{\varepsilon}_i]^2\rangle=\left\langle\left(\sum_{\lambda,\mu}[\boldsymbol{\varepsilon}(\mathbf{k}_-,j)]_\lambda R_a^{\lambda\mu}[\boldsymbol{\varepsilon}_i]_\mu\right)^2\right\rangle, \tag{5.2}$$

$$\langle[\boldsymbol{\varepsilon}(\mathbf{k}_+,j)\cdot\hat{\mathbf{R}}_a\cdot\boldsymbol{\varepsilon}_i][\boldsymbol{\varepsilon}(\mathbf{k}_-,j)\cdot\hat{\mathbf{R}}_a\cdot\boldsymbol{\varepsilon}_i]\rangle$$
$$=\left\langle\left(\sum_{\lambda,\mu}[\boldsymbol{\varepsilon}(\mathbf{k}_+,j)]_\lambda R_a^{\lambda\mu}[\boldsymbol{\varepsilon}_i]_\mu\right)\times\left(\sum_{\lambda',\mu'}[\boldsymbol{\varepsilon}(\mathbf{k}_-,j)]_{\lambda'}R_a^{\lambda'\mu'}[\boldsymbol{\varepsilon}_i]_{\mu'}\right)\right\rangle, \tag{5.3}$$

where the indices $\lambda,\mu,\lambda',\mu'$ run over the laboratory coordinates. Since the elements of the Raman tensor are intrinsic properties of the molecule and are generally expressed by R_a^{pq} with $p,q=X,Y,Z$, we must transform $R_a^{\lambda\mu}$ into the corresponding elements given in the molecular frame

$$R_a^{\lambda\mu}=\sum_{p,q}\Lambda_p^\lambda\Lambda_q^\mu R_a^{pq}, \tag{5.4}$$

with Λ_p^λ and Λ_q^μ the direction cosines between the fixed laboratory axes and the molecule axes. Inserting the (5.4) into the (5.1), we can perform the average by using the evaluations of the direction since averages given in Ref. [17]. Assuming that the Raman tensor is symmetric, the result is

$$\langle(\boldsymbol{\varepsilon}(\mathbf{k}_+,j)\cdot\hat{\mathbf{R}}_a\cdot\boldsymbol{\varepsilon}_i)^2\rangle=\sum_\lambda\left\{\left[\frac{1}{5}\sum_i(R^{ii})^2+\frac{1}{15}\sum_{i\neq j}R^{ii}R^{jj}+\frac{4}{15}\sum_{i\neq j}(R^{ij})^2\right]([\boldsymbol{\varepsilon}(\mathbf{k}_+,j)]_\lambda)^2\right.$$
$$+\sum_\mu^{\mu\neq\lambda}\left[\frac{1}{15}\sum_i(R^{ii})^2-\frac{1}{30}\sum_{i\neq j}R^{ii}R^{jj}+\frac{1}{5}\sum_{i\neq j}(R^{ij})^2\right]([\boldsymbol{\varepsilon}(\mathbf{k}_+,j)]_\mu)^2\Big\}([\boldsymbol{\varepsilon}_i]_\lambda)^2$$
$$+\left[\frac{4}{15}\sum_i(R^{ii})^2+\frac{1}{5}\sum_{i\neq j}R^{ii}R^{jj}+\frac{2}{15}\sum_{i\neq j}(R^{ij})^2\right]\sum_\lambda[\boldsymbol{\varepsilon}(\mathbf{k}_+,j)]_\lambda[\boldsymbol{\varepsilon}_i]_\lambda\sum_\mu^{\mu\neq\lambda}[\boldsymbol{\varepsilon}(\mathbf{k}_+,j)]_\mu[\boldsymbol{\varepsilon}_k]_\mu. \tag{5.5}$$

An analogous result is found for the average (5.2). Equation (5.3) gives instead

$$\langle[\boldsymbol{\varepsilon}(\mathbf{k}_+,j)\cdot\hat{\mathbf{R}}_a\cdot\boldsymbol{\varepsilon}_i][\boldsymbol{\varepsilon}(\mathbf{k}_-,j)\cdot\hat{\mathbf{R}}_a\cdot\boldsymbol{\varepsilon}_i]\rangle$$
$$=\left[\frac{1}{5}\sum_i(R^{ii})^2+\frac{1}{15}\sum_{i\neq j}R^{ii}R^{jj}+\frac{4}{15}\sum_{i\neq j}(R^{ij})^2\right]\sum_\lambda[\boldsymbol{\varepsilon}(\mathbf{k}_+,j)]_\lambda[\boldsymbol{\varepsilon}(\mathbf{k}_-,j)]_\lambda([\boldsymbol{\varepsilon}_i]_\lambda)^2+\left[\frac{1}{15}\sum_i(R^{ii})^2+\frac{2}{15}\sum_{i\neq j}R^{ii}R^{jj}\right.$$
$$\left.-\frac{2}{15}\sum_{i\neq j}(R^{ij})^2\right]\sum_\lambda[\boldsymbol{\varepsilon}(\mathbf{k}_+,j)]_\lambda[\boldsymbol{\varepsilon}_i]_\lambda\sum_\mu^{\mu\neq\lambda}[\boldsymbol{\varepsilon}(\mathbf{k}_-,j)]_\mu[\boldsymbol{\varepsilon}_i]_\mu+\left[\frac{1}{15}\sum_i(R^{ii})^2-\frac{1}{30}\sum_{i\neq j}R^{ii}R^{jj}+\frac{1}{5}\sum_{i\neq j}(R^{ij})^2\right]$$
$$\times\left\{\sum_\lambda[\boldsymbol{\varepsilon}(\mathbf{k}_+,j)]_\lambda[\boldsymbol{\varepsilon}(\mathbf{k}_-,j)]_\lambda\sum_\mu^{\mu\neq\lambda}([\boldsymbol{\varepsilon}_i]_\mu)^2+\sum_\lambda[\boldsymbol{\varepsilon}(\mathbf{k}_+,j)]_\lambda[\boldsymbol{\varepsilon}_i]_\lambda\sum_\mu^{\mu\neq\lambda}[\boldsymbol{\varepsilon}(\mathbf{k}_-,j)]_\mu[\boldsymbol{\varepsilon}_i]_\mu\right\}. \tag{5.6}$$

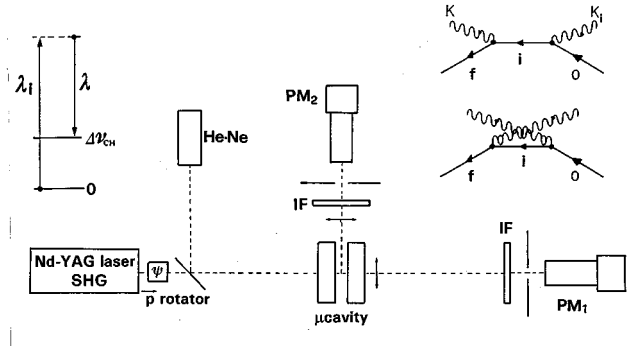

FIG. 2. Layout of the Raman apparatus and Feynman diagrams for electric-dipole interactions in Raman scattering.

Note that the polarizations of the incident (exciting) and of the scattered (measured) fields are expressed in (5.5) and (5.6) by the Cartesian components λ,μ of the unit vectors $\boldsymbol{\varepsilon}_i$ and $\boldsymbol{\varepsilon}(\mathbf{k}_{\pm},j)$, respectively.

Another quantity characterizing the scattering of an anisotropic medium is the ''depolarization ratio'' defined as the ratio between the components $I_{\perp}$ and $I_{\parallel}$ of the scattering intensity polarized in the directions perpendicular and parallel to the incident field polarization $\boldsymbol{\varepsilon}_i$,

$$\rho = I_{\perp}/I_{\parallel}. \tag{5.7}$$

In order to derive its expression, we first note that the intensity I is proportional to the differential cross section

$$I d\Omega = L \frac{d\sigma}{d\Omega} d\Omega \tag{5.8}$$

(L is the incident beam intensity per unitary surface) and then the depolarization ratio is equally given by

$$\rho = \frac{\left(\frac{d\sigma}{d\Omega}\right)_{\perp}}{\left(\frac{d\sigma}{d\Omega}\right)_{\parallel}}. \tag{5.9}$$

The explicit expression of the depolarization ratio depends on the specific molecular parameters. In Sec. VI we give this expression relative to the benzene molecule. Here we just give some very general considerations on the behavior of $\rho(d,\theta)$. Consider the case of an orthogonally injected, vertically polarized incident field with intensity I_i, with the scattering in the horizontal plane occurring with components of the scattered intensity I_v and I_h corresponding, respectively, to a vertically polarized field and to a horizontally polarized field. The ratio I_h/I_v is the depolarization ratio ρ depending on the scattering angle θ. The quantity I_h can be further split along the two horizontal axes y and z of the laboratory frame. We first note that the component I_z is not affected by the confinement. This means that I_h experiences the presence of the cavity only through I_y. Now if we measure the radiation at small scattering angles, $I_h \approx I_y$ and therefore the confinement acts in the same way on I_h and on I_v owing to the cylindrical symmetry of the problem. Their ratio is then unaffected by the microcavity and $\rho/\rho_0 \approx 1$. Suppose now that we measure the radiation at $\theta \approx 90°$. There $I_h \approx I_z$ and the depolarization ratio is completely determined by the confinement acting on I_x. The numerical evaluation takes into account the uniform distribution of the molecules filling the space between the mirrors. Note how the value of d determines the extreme values of ρ. Consider $d < \lambda/2$: both the intensities I_x and I_y are inhibited, while I_z is not. Then ρ is virtually infinite. On the other hand, for a large cavity, i.e., $d \geqslant \lambda/2$, I_x and I_y are determined by the **k**-vector resonances allowed by the cavity. This behavior has been experimentally investigated and the corresponding results are given in Sec. VIII and in Fig. 8.

VI. THE CASE OF BENZENE: NORMAL MODE A_{1g}

The generally theory given in the previous sections will now be applied to the specific case of the benzene molecule, the actual object of our experimental investigation. We will be concerned with the normal vibrational mode A_{1g}, with the Raman shift equal to 3062 cm^{-1}. In this particular case the Raman tensor $\hat{\mathbf{R}}_{A_{1g}}$ is diagonal and can be represented in matrix form as [15]

$$\hat{\mathbf{R}}_{A_{1g}} = \begin{pmatrix} \alpha & 0 & 0 \\ 0 & \alpha & 0 \\ 0 & 0 & \beta \end{pmatrix}, \tag{6.1}$$

where α and β are parameters expressed in terms of products of dipole moment matrix elements relative to virtual transitions among the electronic and vibrational levels of the molecule. They are evaluated by third-order perturbation theory and their explicit, detailed expression is given in Ref. [13]. The presence of unequal elements in the main diagonal of $\hat{\mathbf{R}}_{A_{1g}}$ produces a nonvanishing scattering depolarization ratio, which for a spectroscopically conventional scattering geometry, i.e., in the absence of confinement, is given by the expression

$$\rho_0 = \frac{(\alpha-\beta)^2}{(8\alpha^2+3\beta^2+4\alpha\beta)}. \tag{6.2}$$

It has been found that $\rho_0 = 0.22$ for the liquid phase of benzene at room temperature [18].

By inserting (6.1) into the averaging expression (5.5) and (5.6), we obtain the relative scattering cross section σ/σ_0 for the condition of microcavity confinement and for a polarization of the incident field lying in the (horizontal) plane of observation ($\boldsymbol{\varepsilon}_i$ parallel to y axis; $\psi = 90°$, Fig. 1). For the sake of simplicity, all the given expressions of σ/σ_0 account for the sum of the scattering probabilities relative to the two states of polarization, for each scattering **k** vector. Then

$$\frac{\sigma}{\sigma_0} = \frac{3}{8(1+2\rho_0)} \int_0^1 ((1+\rho_0)\{\chi_{11}(+)+\chi_{21}(-) + C^2[\chi_{12}(+)+\chi_{22}(-)]\} + 2\rho_0(1-C^2)[\zeta_{12}(+)+\zeta_{22}(-)])dC, \tag{6.3}$$

where

$$\chi_{1j}(+)=\frac{|t_{2j}|^2}{|D_j|}\{1+|r_{1j}|^2+2|r_{1j}| \times\cos[k(d+2z)\cos\theta+\phi_{1j}]\}, \quad (6.4)$$

$$\chi_{2j}(-)=\frac{|t_{1j}|^2}{|D_j|}\{1+|r_{2j}|^2+2|r_{2j}| \times\cos[k(d-2z)\cos\theta+\phi_{2j}]\}, \quad (6.5)$$

$$\zeta_{12}(+)=\frac{|t_{22}|^2}{|D_2|}\{1+|r_{12}|^2-2|r_{12}| \times\cos[k(d+2z)\cos\theta+\phi_{12}]\}, \quad (6.6)$$

$$\zeta_{22}(-)=\frac{|t_{12}|^2}{|D_2|}\{1+|r_{22}|^2-2|r_{22}| \times\cos[k(d-2z)\cos\theta+\phi_{22}]\}. \quad (6.7)$$

The calculation of the total cross section corresponding to an incident field depolarization $\boldsymbol{\varepsilon}_i$ parallel to the x axis gives the same result as that inferred from the cylindrical symmetry of the problem. The expression of the depolarization ratio can also be calculated explicitly for the case of cavity confinement. In this case the polarization $\boldsymbol{\varepsilon}(\mathbf{k}_\pm, j)$ of the scattered field is, of course, relevant. Let us evaluate ρ/ρ_0 for the only significant case [19], i.e., the one in which $\boldsymbol{\varepsilon}_i$ is perpendicular to the plane of polarization, the horizontal plane. Then the orthogonal and parallel polarization vectors of the scattered field are

$$\boldsymbol{\varepsilon}_\perp=\boldsymbol{\varepsilon}(\mathbf{k}_\pm,2)=(\cos\theta,0,\mp\sin\theta), \quad (6.8)$$

$$\boldsymbol{\varepsilon}_\parallel=\boldsymbol{\varepsilon}(\mathbf{k}_\pm,1)=(0,-1,0) \quad (6.9)$$

and the depolarization ratio is expressed by

$$\frac{\rho(\theta)}{\rho_0}=\frac{\gamma_{12}(+)+\gamma_{22}(-)}{\chi_{11}(+)+\chi_{21}(-)}, \quad (6.10)$$

where

$$\gamma_{12}(+)=\frac{|t_{22}|^2}{|D_2|^2}\{1+|r_{12}|^2+2(2\cos^2\theta-1)|r_{12}| \times\cos[k(d+2z)\cos\theta+\phi_{12}]\}, \quad (6.11)$$

$$\gamma_{22}(-)=\frac{|t_{12}|^2}{|D_2|^2}\{1+|r_{22}|^2+2(2\cos^2\theta-1)|r_{22}| \times\cos[k(d-2z)\cos\theta+\phi_{22}]\}. \quad (6.12)$$

Note that the expression (6.10) tends to unity as soon as the cavity is removed, i.e,. $r_{1j}=r_{2j}=0$ and $t_{1j}=t_{2j}=1$.

VII. EXPERIMENTAL SETUP

The vibrational transition of the C_6H_6 molecule corresponding to the totally symmetric species A_{1g} with Raman shift $\Delta\nu_{CH}=3026\ \text{cm}^{-1}$ has been investigated under excitation provided by coherent optical pulses at $\lambda_i=532$ nm, with 6 nsec duration and with a repetition rate of 20 pps (Fig. 2).

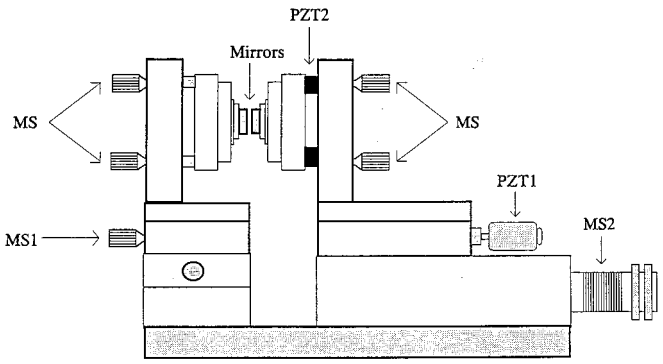

FIG. 3. Detailed microcavity structure without the mirror "bottle" for liquid benzene.

The total energy associated to each excitation pulse was 35 mJ with an energy stability of 3.5%. The beam, with a cross section of 1 cm^2, was generated by a second-harmonic process induced by a Q-switched Nd:YAG laser (where YAG denotes yttrium aluminum garnet) (Continuum, model Surelite). The polarization of the second-harmonic laser beam was controlled by a broadband polarization rotator (Newport, model PR550) inducing a rotation angle ψ, on the plane x-y, of the polarization vector $\boldsymbol{\varepsilon}_i$ of the excitation beam ($\psi=0$ for $\boldsymbol{\varepsilon}_i$ parallel to the vertical x axis). The excitation optical pulse was then injected in the microcavity with a direction $\mathbf{k}_i$ orthogonal to the mirrors. The microcavity spacing was filled with liquid benzene at $T=300$ K. The absence of any stimulated Raman process was verified throughout the experiment by testing the linear dependence of the forward-scattered intensity on the exciting one.

The microcavity consisted of two-plane, equal, circular multilayered-coated mirrors or Bragg reflectors, manufactured by Virgo Optics, Inc. They exhibited a high transparency at the exciting wavelength λ_i and a very high reflection ($R\geqslant 0.998$) at the Stokes wavelength $\lambda=635.5$ nm. The structure of the coatings, deposited over BK7 glass substrates with a diameter of 25.4 mm and planarity greater than or equal to $\lambda/20$, consisted of 25 alternate, unequal thickness h layers made by two semiconductor materials (SiO_2 and Ti_2O_3) with different refractive indices n. The sequence of the h values, given in units of 10^{-1} μm, was [glass–L'' 1.49–12×(H'' 2.27–L'' 1.49)–air]. The label L'' represents SiO_2, $n=1.49$ at 632.8 nm while H'' represents Ti_2O_3, $n=2.27$ at the same wavelength. The optical parameters of the mirrors, i.e., reflectivity $R(\theta)$ and phase $\phi(\theta)$, were accurately determined by an extensive computer calculation based on the Lisberger-Wilcock algorithm [20], which we tested in another work [10].

Since the main purpose of this work is to investigate the dependence of the relevant scattering parameters on the size d of the microcavity, this one had to be adjusted in a precise and controllable way at "microscopic" values comparable with the Stokes wavelength $\lambda=635.5$ nm. For this purpose, the mirror holders were mounted over two independent micrometric slides (MSS) allowing fine adjustments along the optical axis of the system (Fig. 3). One of these (MSI) was controlled manually with an accuracy of 10 μm. The other (MS2) was driven by a step-by-step displacer (Micro-Controle, model UT 50.20 PP) having a translation resolu-

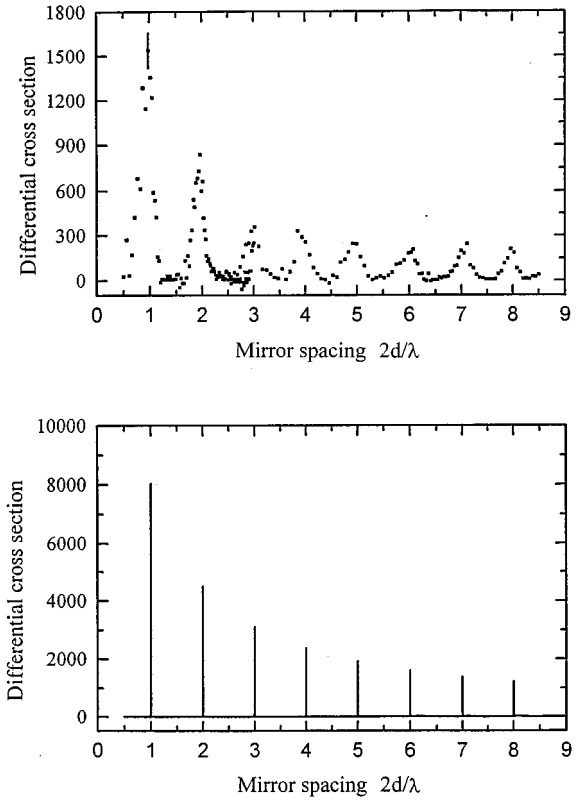

FIG. 4. Differential cross section $(d\sigma/d\Omega)/(d\sigma/d\Omega)_0$ relative to the corresponding free-space value as a function of the mirror spacing d for the confined Raman scattering in C_6H_6 and for the A_{1g} mode with $\Delta\nu_{CH}=3062$ cm^{-1} (Stokes wavelength $\lambda=635.5$ nm). The lower plot expresses the results of the theory.

tion of 1000 Å and controlled by an electronic driver (Micro-Controle, model IT 6D CA 1). In addition, a finer motion of translation was ensured by a piezoelectric pusher (Burleigh, model PZ-30, indicated as PZT1 in Fig. 3), which provided a total motion of 5 μm for an applied voltage of 1 kV. The applied voltage feeding the PZT1 transducer was controlled by a computer. This allowed a high-precision scanning of the mirror distance over few Stokes wavelengths.

Consideration of the thermal expansions of the material forming all the overall cavity structure was found to be important in the context of our high-precision measurement. The material chosen for the realization of the cavity structure was steel AISI 410 having a coefficient of linear expansion of 10.3×10^{-6} K^{-1}. The high thermal stability of the overall system was also determined by an accurate air-temperature control of the laboratory for the whole duration of the measure. The condition of thermal stability, the alignment of the Fabry-Pérot cavity (i.e, the parallelism of the mirrors), and, most important, the absolute value d of the cavity spacing were determined by repeated observations, during the experiment, of the interference Airy transmission peaks generated by a cw, *on-line*, He-Ne laser. This one was injected orthogonally onto the cavity and detected through the sideband of an interference filter, centered on $\lambda=635.5$ nm with bandwidth $\Delta\lambda=0.3$ nm. This filter was placed in front of the same photomultiplier (RCA, model C31034A-02, PM_1 of Fig. 2) that was used to detect the Raman-Stokes light in condition of pulsed excitation. The fine alignment of the mirrors was

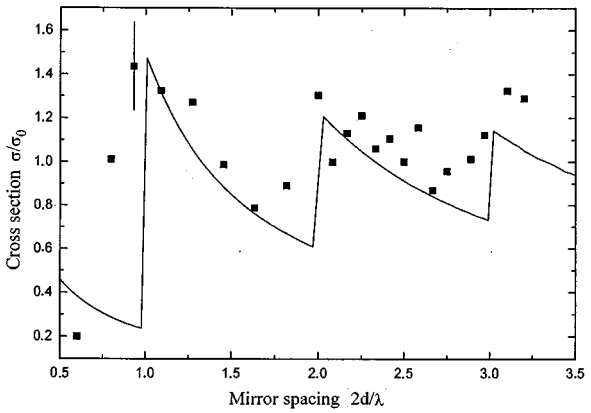

FIG. 5. Total Raman cross section (σ/σ_0) relative to the free-space value as a function of the cavity spacing d for the confined scattering at $\lambda=635.5$ nm.

also ensured by two computer-controlled piezoelectric pushers (PZT2) connected with the mirror holders. In order to avoid the evaporation of the liquid C_6H_6 in the microcavity, we had to conceive of a kind of an elastic, very light cylindrical bottle sealed on the circular sides of the mirrors.

The intensity of the scattered radiation detected by the photomultiplier was measured by a photon-counting technique by using a SR400 Stanford Research System gated counter. The counting gate was set to 200 nsec and the data were handled by a computer. The scattered light emitted by the microcavity in *transverse* directions was detected by a second phototube PM_2. By a precision optical system, the Stokes photons diffracted by the borders of the mirrors were focused on the cathode of PM_2. There again, the photon-counting technique was adopted.

VIII. EXPERIMENTAL RESULTS

A. Cross section

The confined Stokes radiation at λ was detected in the forward direction $\theta=0$ over a solid angle $\Delta\Omega=1.3\times10^{-4}$ sr. The scattering data obtained in vacuum-confinement condition, i.e, for a ''microscopic'' value of the cavity dimension $d\approx\lambda$, were compared with the ''free-space'' values obtained in absence of the cavity mirrors, i.e,. with mirror reflectivities $R\cong0$. We found that free-space condition was well approximated by setting d at ''macroscopic'' values $d\geqslant10^3\lambda$.

The dependence on d on the *differential cross section*, evaluated along the axial z direction, is shown in Fig. 4. The results show a dramatic enhancement for increasing confinement (i.e., for decreasing d) of the peaks of $(d\sigma/d\Omega)$ appearing for $d=n\lambda/2$, with n a whole number greater than 1.

The most dramatic effect of confinement on the scattering redistribution shown by Fig. 4 comes with a still more important phenomena. As shown by Fig. 5 the *total scattering cross section*, i.e, the emission probability over *all channels*, is also largely affected by the confinement process. We see, for instance, that for $d\approx\lambda/2$ any single molecule scatters over all angles about 1.5 times more efficiently than in free space, while for $d<\lambda/2$ the overall scattering process is strongly inhibited: there the molecular dipole is ''frozen'' for this particular Raman mode.

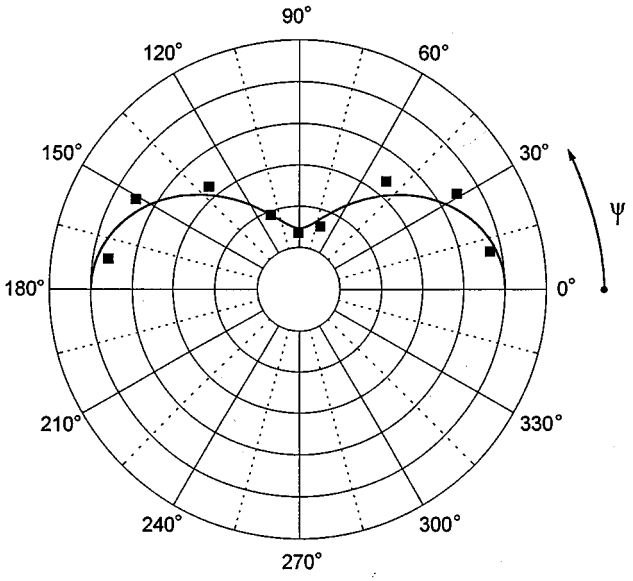

FIG. 6. Angular dependence of the scattered intensity emitted in the transverse microcavity plane $z=0$ along the y axis. The reported intensity distribution is relative to the angle ψ between the exciting field polarization $\boldsymbol{\varepsilon}_i$ and the x axis in the transverse plane.

The experimental data of (σ/σ_0), reported in Fig. 5, represent the most important result of the present work. They also correspond to the hardest experimental challenge faced during the work. Each experimental point of Fig. 5 was the result of several combined detection and photon-counting experiments carried out with both phototubes PM_1 and PM_2 and lasting hours. By the phototube PM_1, the Stokes intensity was detected in the forward direction, with different scattering angles θ and with different acceptance angles $\Delta\Omega$ of the detector. By the phototube PM_2 the Stokes intensity was detected in transverse directions. Consider that, in order to obtain a consistent datum at a certain value of d, a very large stability of the overall experimental conditions had to be attained, namely, the laser intensity, the thermal drift of the cavity, the stability of the electronics, etc. Note also that the overall experiment, i.e., carried out for different values of d, lasted days. Then the consistency of the data reported in Fig. 5 still required an exceptional experimental stability and a careful control over all parameters.

The theoretical plot of the total cross section, also shown in Fig. 6 as a solid line, has been determined by numerical evaluation of the integral (6.3) with a further integration to account for the isotropic molecular orientations. We note that the difference with the experimental data is less evident than that one reported in Fig. 5 for $d\sigma/d\Omega$. This may be due to the larger insensitivity of the total cross section σ on the reflectivities of the mirrors and on the spacing d. The former effect reduces the influence of the imperfections of the mirrors, which lower the value of the cavity finesse, while the latter reduces the errors coming from the instability on d.

The angular ψ distribution of the overall scattering intensity emitted in the transverse microcavity plane $z=0$, i.e., with $\theta=90°$, has been investigated by changing the angle ψ of the injected pump-polarization vector $\boldsymbol{\varepsilon}_i$ (Fig. 6). We found that the overall scattering intensity in transverse direction for $d=\lambda/2$ is about 1% of the total emission.

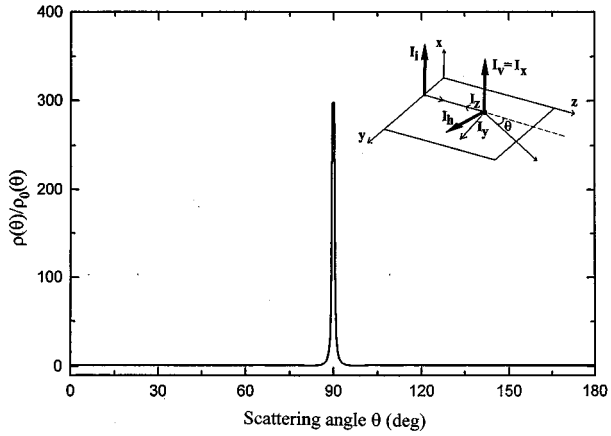

FIG. 7. Angular dependence of the depolarization ratio (ρ/ρ_0) relative to the free-space value in the horizontal plane (y-z) for a vertical direction of the incident polarization $\boldsymbol{\varepsilon}_i$ ($\psi=0$) and for a cavity dimension of $5\lambda/2$. The geometry of the scattering kinematics is reported in the inset: refer to the text for a description.

B. Depolarization ratio

The angular dependence of the depolarization ratio (ρ/ρ_0) relative to the free-space value in the horizontal plane for vertical incident polarization $\boldsymbol{\varepsilon}_i(\psi=0)$ is reported in Fig. 7. Note the strong confinement effect at $\theta=90°$, in agreement with the theoretical discussion given in Sec. V. A strong confinement effect for the scattering depolarization ratio at $\theta\approx 90°$ vs the mirror spacing d is shown in Fig. 8. The data show that the effect of confinement is gradually attenuated toward the free-space value $\rho(90°)/\rho_0(90°)=1$ for large d's. The corresponding theoretical plot (solid line) is also shown. It has been derived by integrating the result of Eq. (6.10) over a randomly oriented distribution of excited molecules and for a finite diameter of the mirrors.

IX. CONCLUSIONS

We have reported a rather extensive investigation of spontaneous Raman scattering in the microscopic Fabry-Pérot cavity. The theory is based on the complete set of modes described by (2.7) and (2.8). The main result is the expression (4.6) of the total cross section for a random, oriented

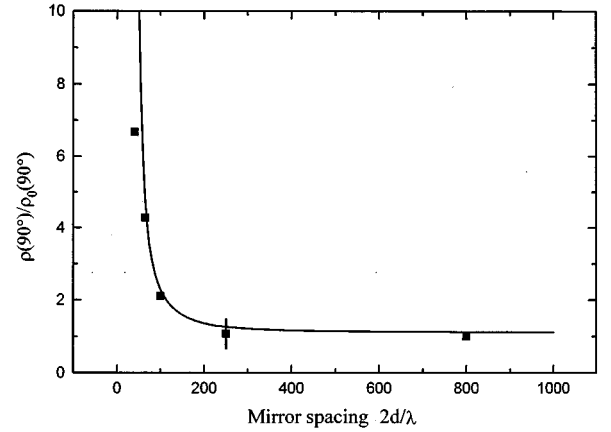

FIG. 8. Depolarization ratio at 90° relative to the free-space value as a function of the mirror spacing d.

molecule. The case of the Stokes shift at 3062 cm^{-1} in a liquid sample of benzene has been taken as paradigmatic and the total cross section has been calculated and measured. Experimental results showing the strong confinement effect have also been given for two directional properties such as the differential cross section and the depolarization ratio.

The reported processes are expected to be of relevance in the field of atomic and molecular spectroscopy. For instance, spectra of (electric-dipole) ''Raman-inactive'' modes (i.e., involving high-order multipole transitions) or hyper-Raman transitions could be made observable by our technique. In other nonlinear optics effects, the striking modification of the scattering parameters will certainly lead to a ''thresholdless'' high-gain behavior of the stimulated process in microparametric or microlaser devices [6,21].

A feature of general relevance must be considered in the Casimir vacuum-confinement process described above. Enhancement and inhibition effects similar to the reported ones are expected to be generally reproduced by other QED scattering processes involving photon emission [22]. Examples could, in principle, be given by the Compton scattering, matter-antimatter pair annihilation or other scattering processes in high-energy physics. As a further example, our enhancement scheme could virtually represent the key solution in the experiment aimed at the demonstration of the parametric photon-photon interaction via the high-order QED, nonlinear polarization [23].

ACKNOWLEDGMENTS

We acknowledge useful conversations with Francesco Cairo, Daniele Murra, Rodney Loudon, and Salvatore Califano.

[1] J. Bjorken and S. Drell, *Relativistic Quantum Mechanics* (McGraw-Hill, New York, 1964), Chap. 6.

[2] E. M. Purcell, Phys. Rev. **69**, 681 (1946).

[3] H. Morawitz, Phys. Rev. **187**, 1792 (1969); M. R. Philpott, Chem. Phys. Lett. **19**, 435 (1973); C. H. Townes and A. Schawlow, *Microwave Spectroscopy* (McGraw-Hill, New York, 1955), p. 336; J. R. Ackerhalt, P. L. Knight, and J. H. Eberly, Phys. Rev. Lett. **30**, 456 (1973); J. Ackerhalt and J. H. Eberly, Phys. Rev. D **10**, 3350 (1974); I. R. Senitzky, Phys. Rev. Lett. **31**, 995 (1973); P. W. Milonni, J. R. Ackerhalt, and W. A. Smith, *ibid.* **31**, 958 (1973); D. Kleppner, *ibid.* **47**, 233 (1981); J. Dalibard, J. Dupont-Roc, and C. Cohen Tannoudij, J. Phys. **43**, 1617 (1982); E. T. Jaynes, in *Coherence and Quantum Optics*, edited by L. Mandel and E. Wolf (Plenum, New York, 1978); L. Allen and J. H. Eberly, *Optical Resonance and Two-Level Atoms* (Dover, New York, 1975), Chap. 7.

[4] P. Goy, J. Raimond, M. Gross, and S. Haroche, Phys. Rev. Lett. **50**, 1903 (1983); R. G. Hulet, E. S. Hilfer, and D. Kleppner, *ibid.* **55**, 2137 (1985); D. Meschede, H. Walther, and G. Muller, *ibid.* **54**, 551 (1985). For a review on spontaneous emission effects with Rydberg atoms, see P. Filipowicz, P. Meystre, G. Rempe, and H. Walther, Opt. Acta **32**, 1105 (1985); G. Gabrielse and H. Dehmelt, Phys. Rev. Lett. **55**, 67 (1985); W. Jhe, A. Anderson, E. A. Hinds, D. Meschede, L. Moi, and S. Haroche, *ibid*. **58**, 666 (1987), reported spontaneous emission microcavity work in the near infrared ($\lambda = 3.59$ μm) with a cw technique; D. J. Heinzen, J. J. Childs, J. E. Thomas, and M. S. Feld, *ibid.* **58**, 1320 (1987).

[5] K. H. Drexhage, in *Progress in Optics*, edited by E. Wolf (North-Holland, Amsterdam, 1974), Vol. 12; F. De Martini, Phys. Lett. A **115**, 421 (1986).

[6] F. De Martini and G. Innocenti, in *Quantum Optics IV*, edited by J. Harvey and F. Walls (Springer, Berlin, 1986), F. De Martini and G. Innocenti (unpublished); F. De Martini, G. Innocenti, G. R. Jacobovitz, and P. Mataloni, Phys. Rev. Lett. **59**, 2955 (1987). The quasithresholdless dynamics in the microlaser was reported by F. De Martini and G. R. Jacobovitz, *ibid.* **60**, 1711 (1988); F. De Martini, Phys. Scr. **21**, 58 (1988), F. De Martini, F. Cairo, P. Mataloni, and F. Verzegnassi, Phys. Rev. A **46**, 4220 (1992). The transverse interatom quantum correlations in the active microcavity were investigated by F. De Martini, M. Marrocco, and D. Murra, Phys. Rev. Lett. **65**, 1853 (1990).

[7] For theoretical Raman investigation regarding some important nonclassical phenomena, see, for example, C. C. Gerry and J. H. Eberly, Phys. Rev. A **42**, 6805 (1991); G. S. Agarwal and R. R. Puri, *ibid.* **43**, 3949 (1991); C. C. Gerry and H. Huang, *ibid.* **45**, 8037 (1992); C. K. Law and J. H. Eberly, *ibid.* **47**, 3195 (1993).

[8] E. B. Wilson, J. C. Decius, and P. C. Cross, *Molecular Vibrations* (McGraw-Hill, New York, 1955), Chap. 10.

[9] F. Cairo, F. De Martini, and D. Murra, Phys. Rev. Lett. **70**, 1413 (1993).

[10] F. De Martini, M. Marrocco, P. Mataloni, L. Crescentini, and R. Loudon, Phys. Rev. A **43**, 2480 (1991).

[11] R. Loudon, *The Quantum Theory of Light*, 2nd ed. (Oxford University Press, New York, 1983).

[12] A. C. Albrecht, J. Chem. Phys. **34**, 1476 (1961).

[13] W. L. Peticolas, L. Nafie, P. Stein, and B. Fanconi, J. Chem. Phys. **52**, 1576 (1970).

[14] J. J. Sakurai, *Modern Quantum Mechanics* (Benjamin/Cummings, Reading, MA, 1985), Chap. 5; a detailed argument is given in Ref. [13].

[15] L. Nafie, P. Stein, B. Fanconi, and W. L. Peticolas, J. Chem. Phys. **52**, 1584 (1970); R. Loudon., Adv. Phys. **13**, 423 (1964).

[16] Y. Kato and H. Takuma, J. Chem. Phys. **54**, 5398 (1971).

[17] S. J. Cyvin, J. E. Rauch, and J. C. Decius, J. Chem. Phys. **43**, 4083 (1965).

[18] H. Mikosch, J. Mol. Struct. **218**, 243 (1990).

[19] J. H. Hibben, *The Raman Effect and its Chemical Application* (Reinhold, New York, 1939), Chap. 4.

[20] P. H. Lissberger, J. Opt. Soc. Am. **49**, 121 (1959); P. H. Lissberger and W. L. Wilcock, *ibid.* **49**, 126 (1959).

[21] W. Hsieh, J. Zheng, and R. K. Chang, Opt. Lett. **13**, 497 (1988); H. Lin, A. Huston, J. D. Eversole, and A. J. Campillo, J. Opt. Soc. Am. B **7**, 2079 (1990).

[22] G. Plunien, B. Muller, and W. Greiner, Phys. Rep. **134**, 89 (1986).

[23] C. Itzykson and J. Zuber, *Quantum Field Theory* (McGraw-Hill, New York, 1980), Chap. 3; J. McKenna and P. M. Platzman, Phys. Rev. **129**, 2354 (1962).